Manipulation of Majorana zero-modes using double quantum dots

Jesus D. Cifuentes[1] and Luis G. G. V. Dias da Silva[1]

[1] *Instituto de Física, Universidade de São Paulo, C.P. 66318, 05315–970 São Paulo, SP, Brazil*

(Dated: April 2, 2019)

Majorana zero modes (MZMs) emerging at the edges of topological superconducting wires are a promising platform for fault-tolerant quantum computation. Novel proposals use quantum dots (QDs) coupled to the end of these wires to detect Majorana signatures. This detection method provides the following advantages: 1) This device allows to study the prospective coexistence of Kondo-Majorana signatures, which have been recently reported in experiments. 2) Today's precise experimental control over QDs offers the unique possibility of manipulating MZMs inside multi-dot systems, which recently enlightened the design of scalable quantum architectures.The simplest case where Majorana manipulation is possible is in a double quantum dot (DQD). This model offers several possibilities for manipulation of MZMs, including different geometric configurations of the dots, from symmetric and linear couplings to T-dot junctions. In this project we perform analytical (non-interacting) and numerical(interacting) quantum transport studies of the transition of the Majorana signature. By tuning the model parameters we show that it is possible to control the localization of the MZM inside the DQD.

I. INTRODUCTION

The pursuit of Majorana quasi-particles in topological superconductors has attracted significant attention in the last decades[1,2]. Since the first Kitaev's toy models[3,4] claiming promising applications to quantum computing, the field evolved rapidly towards physical realizations of the Kitaev chain. The last few decades have been full of excitement as new technological innovations allowed to document several times the observation of Majorana signatures[5–10]. One of the most promising structures is the so-called Majorana wire, which recipe consists in growing semiconducting wires with strong-orbit-coupling over proximity-induced topological (p-wave) superconductors.

These signatures are characterized by the emergence of robust zero modes localized at the edges of the material. However the observed Majorana zero-modes (MZM) have been found in superposition with other similar types of phenomenon such as the Kondo effect[11]. The new experimental proposals foucus on distinguishing MZMs from other effects and performing braiding protocols[12–14], a basic operation for topological quantum computing.

A promising method to detect MZMs consists in attaching a quantum dot (QD) to the edges of a Majorana chain in the topological phase and executing transport measurements through the QD.[15] In such arrangement the MZM at the end of the chain leaks inside the ,QD[16] which produces a zero-bias conductance peak of half a quanta $\frac{e^2}{2h}$ through the dot. Recently, experiments including hybrid Majorana-QD systems have been performed.[9] This method offers several advantages: 1) The qubit information is not completely destroyed, in contrast to other detection methods such as tunneling spectroscopy. 2) If performed under the Kondo temperature T_k it allows the possibility of observing the MZM co-existing with the Kondo peak,[17–19] and methods for separating both effects 3) Today's precise experimental control over the QD parameters offers the unique possibility of manipulating MZMs inside multi-dot systems. Hence bringing new lights into the design of quantum architectures[20,21].

The simplest case where Majorana manipulation is possible is in a double quantum dot (DQD). Tunneling Majorana modes in these basic structures have inspired theoretical studies[22,23] and experimental setups confirming the observations of Andreev molecules[24]. Even though quantum tunneling of a MZM into a double dot offers several possibilities for manipulation of MZM, there is still no complete analysis of the transitions of the Majorana signatures between the QDs in this model.

In this paper, we explore the different possibilities for Majorana manipulation in a device consisting of a DQD coupled to a MZM and a metallic lead (See Fig. 1). The simplicity of this model allows us to explore analytically different geometries of QD's from linear couplings to T-junctions (Fig. 2). We considered both non-interacting and interacting regimes, observing major agreement between both approaches about the location of the Majorana signature.

We performed a detailed study of the non-interacting DQD limit, by using Zubarev's procedure[25] to provide an exact formula to calculate the spectral functions. For the interacting case, we resort to numerical renormalization group (NRG)[26] calculations for this model. While the non-interacting regime is suitable to obtain exact expressions for the Green function, the interacting case shows how the Majorana signature co-exists with strongly correlated phenomena such as the Kondo effect[27] and RKKY interactions.[28–30]

This paper is organized as follows. In Sec. II we describe the model of a DQD coupled to a MZM and to a metallic lead, as well as the methods used. The results are presented in section III where we compare the non-interacting density of states (LDOS) III A with the low-energy interacting results III B. Finally, our conclusions are given in Sec. IV.

II. MODEL AND METHODS

We consider the setup shown in Figure 1, in which a single MZM γ_1 located at the edge of a 1D topological superconductor is coupled to a double quantum dot (DQD) attached to a single metallic lead. The Hamiltonian of the entire system can be expressed as:

$$H = H_{\rm DQD} + H_{\rm lead} + H_{\rm DQD-lead} + H_{\rm M-DQD} \qquad (1)$$

where the different terms describe, respectively, the (interacting) DQD, the (non-interacting) metallic lead, and the DQD-lead and DQD-MZM couplings:

$$\begin{aligned} H_{\rm DQD} =& \sum_{\substack{i=1,2\\ \sigma=\downarrow,\uparrow}} \left(\epsilon_{di} + \frac{U_i}{2}\right)\hat{n}_{i\sigma} + \frac{U_i}{2}\left(\sum_{\sigma}\hat{n}_{i\sigma} - 1\right)^2 \\ &+ \sum_{\sigma} t_{dots}(d^\dagger_{1\sigma}d_{2\sigma} + d^\dagger_{2\sigma}d_{1\sigma}) \ , \\ H_{\rm lead} =& \sum_{\mathbf{k}\sigma} \epsilon_{\mathbf{k}} c^\dagger_{\mathbf{k}\sigma} c_{\mathbf{k}\sigma} \ , \\ H_{\rm DQD-lead} =& \sum_{\mathbf{k}\sigma}\sum_{i=1,2} V_{i\mathbf{k}} c^\dagger_{\mathbf{k}\sigma} d_{i\sigma} + V^*_{i\mathbf{k}} d^\dagger_{i\sigma} c_{\mathbf{k}\sigma} \ , \\ H_{\rm M-DQD} =& \sum_{i=1}^{2} t_i \left(d^\dagger_{i\downarrow}\gamma_1 + \gamma_1 d_{i\downarrow}\right) \ . \end{aligned} \qquad (2)$$

In the equations above, ϵ_{di} is the energy level of dot i, U_i is the Coulomb repulsion and t_{dots} is the coupling parameter between both QDs. The operator $d^\dagger_{i\sigma}$ creates a particle in dot i with spin σ and $\hat{n}_{i\sigma} := d^\dagger_{i\sigma} d_{i\sigma}$ is the particle number operator of state i. $c^\dagger_{\mathbf{k}\sigma}$ is the creation operator a particle with momentum $\mathbf{k}$ and spin σ in the lead. $\epsilon_{\mathbf{k}l}$ is the corresponding energy and $V_i(\mathbf{k})$ describes the tunneling coupling between the lead and dot i .

It is sometimes useful to recast the last term in Eq. (1) in terms of (Dirac) fermionic operators. Following Refs. 17 and 18, we choose to write the Majorana zero modes γ_1 and γ_2 as a superposition of the creation ($f^\dagger_\downarrow$) and annihilation ($f_\downarrow$) operators of a spin $\downarrow$ fermion:

$$\gamma_1 := \frac{1}{\sqrt{2}}\left(f^\dagger_\downarrow + f_\downarrow\right) \ , \gamma_2 := \frac{i}{\sqrt{2}}\left(f^\dagger_\downarrow - f_\downarrow\right) \ . \qquad (3)$$

In this representation, the effective coupling between the MZM γ_1 and the DQD becomes:

$$H_{\rm M-DQD} = \sum_i t_i \left(d^\dagger_{i\downarrow} f^\dagger_\downarrow + f_\downarrow d_{i\downarrow} + d^\dagger_{i\downarrow} f_\downarrow + f^\dagger_\downarrow d_{i\downarrow}\right) \qquad (4)$$

where t_i is the coupling parameter between the Majorana mode and QD i.

For the purposes of identifying the presence/absence of MZMs "leaking" from the edge of the TS into the dots[15,16,18], the quantities of interest are the spin-resolved spectral functions (or, equivalently, the local density of states) of the quantum dots. As usual, the spectral function for spin σ in dot i is defined as:

$$\rho_{i\sigma}(\omega) \equiv -\frac{1}{\pi}{\rm Im}\left[G_{d_{i\sigma},d^\dagger_{i\sigma}}(\omega)\right] . \qquad (5)$$

where $G_{d_{i\sigma},d^\dagger_{i\sigma}}(\omega) \equiv \langle\langle d_{i\sigma}, d^\dagger_{i\sigma}\rangle\rangle_\omega$ is the retarded (diagonal) Green's function involving dot i operators $d_{i\sigma}$ and $d^\dagger_{i\sigma}$. Next, we describe the procedures for calculating $\rho_{i\sigma}(\omega)$ in the regimes of weak ($U_i \ll V$) and strong ($U_i \gg V$) electron-electron interaction in the dots.

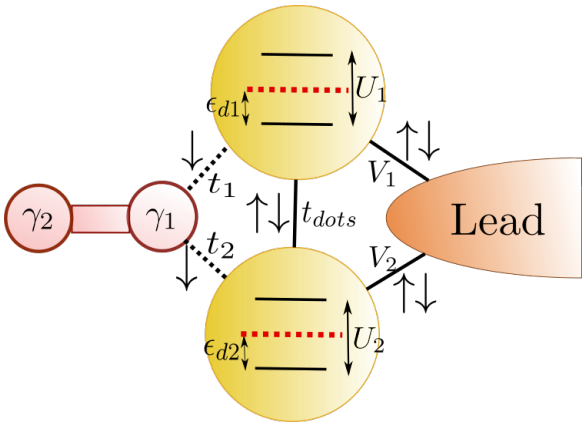

FIG. 1. Model for the DQD-Majorana system. Solid lines: Hopping interactions (t_{dots}: inter-dot coupling , V_1, V_2 couplings of QD1 and QD2 with the lead.). Dashed lines: Majorana spin-$\downarrow$ effective couplings (4) t_1, t_2. The atomic energy levels appear inside each QD ϵ_1, ϵ_2 are tuned by the gate voltages. The coulomb interaction is represented by U_1, U_2. The red dashed horizontal lines represent the Fermi level.

A. Non-interacting limit: Equations of motion

In the non-interacting limit ($U_i = 0$), we can obtain analytic expressions for the spectral densities defined in Eq. (5). Using Zubarev's equation of motion (EOM) approach[25], we can derive exact expressions for the Green functions associated to both quantum dot operators ($G_{d_1 d^\dagger_1}(\omega), G_{d_2 d^\dagger_2}(\omega)$).

The EOM equations define a 9×9 linear system where the Hamiltonian parameters ($t_1, t_2, \epsilon_1 \ldots$) and the energy ω are taken as algebraic variables. The solution for these types of equations is a polynomial fraction of the same degree, which makes it difficult to provide an exact solution using either analytic or numerical methods. To bypass this problem, we introduced a Graph-Gauss-Jordan elimination process[31] to iteratively solve the coupled equations of motion. We briefly describe the procedure here.

We begin by representing the Majorana-DQD quantum dot system in a "flow graph", where each spin-resolved fermionic operator (e.g. $d^\dagger_{1\downarrow}$, $d_{1\downarrow}$, $f_\downarrow$, $f^\dagger_\downarrow$, etc.) is represented as a "vertex" while the coupling terms involving

two fermionic operators (such as $d^\dagger_{1\downarrow} f_\downarrow$ or $d^\dagger_{1\downarrow} f^\dagger_\downarrow$, etc.) are represented as "lines" connecting the respective vertices (see Fig. 10). We then proceed to iteratively eliminating vertices and lines by rewriting the "target" Green's functions in terms of self-energies and other target GFs. In the end, we are left with a linear system for the target Green's functions, which can be directly solved.

This method proved to be efficient in solving complex systems of coupled Green's functions since the graph structure allows us to identify minimum cutting points and create an algorithmic representation Luis ??? of the Green function. A more detailed description is given in Appendix A.

Luis *We need to define what exactly is " an algorithmic representation of the Green function."*

After applying the Graph-Gauss-Jordan process, we obtain a closed form for the non-interacting Green's functions. For instance the GF for dot 1 (which is directly coupled to the MZM) will be given by:

$$G_{d_{1\downarrow},d^\dagger_{1\downarrow}}(\omega) = \frac{1}{\omega - \epsilon^+_{DQD} - \frac{\|T_+\|^2}{\omega-\epsilon_{M2} - \frac{\|T_-\|^2}{\epsilon^-_{DQD}}}}, \quad (6)$$

where the poles are given by

$$\epsilon^\pm_{DQD} = \pm\epsilon_1 + \sum_{\mathbf{k}} \frac{V_1 V_1^*}{\omega-\epsilon_{\mathbf{k}}} + \frac{\left\|\pm t_{dots} + \sum_{\mathbf{k}} \frac{V_1 V_2^*}{\omega-\epsilon_{\mathbf{k}}}\right\|^2}{\omega \pm \epsilon_2 - \sum_{\mathbf{k}} \frac{V_2 V_2^*}{\omega-\epsilon_{\mathbf{k}}}}, \quad (7)$$

$$T_\pm = \pm t_1 \pm t_2 \frac{\left(\pm t_{dots} + \sum_{\mathbf{k}} \frac{V_1 V_2^*}{\omega-\epsilon_{\mathbf{k}}}\right)}{\omega \pm \epsilon_2 \pm \sum_{\mathbf{k}} \frac{V_2 V_2^*}{\omega-\epsilon_{\mathbf{k}}}}, \quad (8)$$

and

$$\epsilon_{M2} = \omega - \epsilon_M - \frac{\frac{\omega}{\omega+\epsilon_M}\|t_2\|^2}{\omega - \epsilon_2 - \sum_{\mathbf{k}} \frac{V_2 V_2^*}{\omega-\epsilon_{\mathbf{k}}}} - \frac{\frac{\omega}{\omega+\epsilon_M}\|t_2\|^2}{\omega + \epsilon_2 - \sum_{\mathbf{k}} \frac{V_2 V_2^*}{\omega+\epsilon_{\mathbf{k}}}}. \quad (9)$$

The spin-↑ LDOS, which is *not* coupled to the MZM, can be obtained by taking $t_1, t_2 = 0$ in Eqs. (10)-(9), hence giving

$$G_{d_{1\uparrow},d^\dagger_{1\uparrow}}(\omega) = \frac{1}{\omega - \epsilon^+_{DQD}}. \quad (10)$$

The final results will depend on the broadening parameter of QD i with the lead (Γ_i), given, in the broad-band limit, by:

$$-i\Gamma_i = \lim_{s\to 0} \sum_{\boldsymbol{k}} \frac{V_i^* V_i}{\omega + is - \epsilon_{\boldsymbol{k}}}. \quad (11)$$

By convention we take Γ_1 as the energy unit for the rest of the project. Finally, we compute the spin-resolved LLDOS in dot 1 as:

$$\rho_{1\sigma}(\omega) = -\frac{1}{\pi}\mathrm{Im}\left[G_{d_{1\sigma},d^\dagger_{1\sigma}}(\omega))\right]. \quad (12)$$

Similar results can be obtain for the LDOS of the second $\rho_{2\sigma}$ by exchanging the indexes 1 and 2 in Eq. (10).

B. Interacting limit: Wilson's NRG

In order to address the case of *interacting* quantum dots, we employ the Numerical Renormalization Group (NRG), one of the most successful methods used to study interacting quantum impurity models (QIMs)[26,32,33]. In general, a QIM describes a system spanning a finite and relatively small Hilbert space (the "impurity") coupled to a much larger system (a "continuum"), spanning a large (typically infinite) Hilbert space. As it turns out, the Hamiltonian in Eq. (1) can be cast as a QIM where the impurity is the DQD coupled to the Majorana mode, which is then coupled to the continuum of electrons in the metallic leads.

We notice that the DOQ-Majorana tunneling term given by Eq. (4) effectively breaks total spin S_z and charge Q conservation of the whole system, while it preserves spin-↓ parity $P_\downarrow = \pm 1$ and spin up particle number $N_\uparrow$. To improve the efficiency of the method, we used these symmetries to maintain a block structure during NRG's iterative diagonalization process[17,18,26]. Both the states serving as a basis for the initial impurity Hamiltonian and the single-site Wilson chain states can be grouped in $(N_\uparrow, P_\downarrow)$ blocks. Thus, the $(N_\uparrow, P_\downarrow)$ block structure is preserved during the entire NRG iteration process[26]. In order to compute the (interacting) spectral functions, we use the density matrix renormalization group (DM-NRG)[34] in combination with the z-trick method[35], which improves spectral resolution at high energies. We have checked the accuracy of the results by comparing the results with the Complete Fock Space method[36] for some of the parameters used.

III. RESULTS

For the remainder of the paper, we will focus on the Majorana-DQD coupling geometries depicted in Fig. 2: a "symmetric coupling" arrangement (Fig. 2-a), a ' "T-shaped" configuration (Fig. 2-b) and the case where the Majorana and the both dots are coupled "in-series" (Fig. 2-c). As we shall see, the intensity of the MZM signature in each dot can be controlled by external gate-voltages which change the position of the dot levels $\epsilon_{1,2}$ relative to the Fermi energy in the leads.

As mentioned previously, the spin-resolved spectral density (or local density of states LLDOS) of each quantum dot provides significant information about the effective tunneling (or not) of a Majorana zero mode into the dot. By comparing the spectral densities for the cases with and without DQD-Majorana couplings, we could identify two generic types of signatures of the Majorana presence in the quantum dots, as follows:

- **Type I:** The spin-↓ LLDOS is half of the spin-↑ LDOS at the Fermi energy ($\rho_\downarrow(0) = \rho_\uparrow(0)/2$).
- **Type II:** The spin-↓ spectral density shows a zero

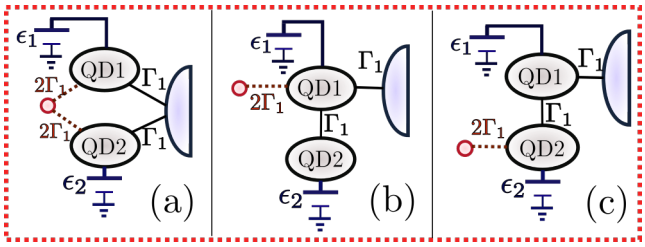

FIG. 2. (a) Symmetric coupling of the DQD to the lead and the MZM. No inter-dot coupling. (b) T-dot arrangement. (c) Quantum dots coupled in series.

mode of height $\rho_\downarrow(0) = \frac{0.5}{\pi\Gamma_1}$ while no such signature appears in the spin-↑ spectral density.

As we shall see in the following Sections, these two types of signatures appear over a wide range of parameters in our results. Type I often appears when there is a zero-mode in the spin-↑ LLDOS while Type II typically emerges in when such a spin-↑ mode is destroyed. Luis *Need to clarify "destroyed"*

Hereafter, we shall refer to "MZM manipulation" the changes in the Majorana signatures in the dot spectral functions induced by the tuning of the dot gate voltages (ϵ_1, ϵ_2) in the three different setups depicted in Fig.2. In each case, we consider definite values of the couplings Γ_2, t_{dots}, t_1 and t_2, as follows. In the configuration shown in Fig.2-(a), we coupled the QD symmetrically to the lead and the MZM by setting $t_1 = t_2$. Within this setup, we expect the MZM signature to "split" due to quantum interference and identical signatures should appear in the spectral densities of both dots. We also considered setups in which only one of the dots is coupled directly the MZM or to the metallic lead. Hence, there are only two distinct coupling geometries: either both the MZM and the lead are coupled to the same dot, forming a "T-junction" or "side-dot" configuration ($t_{2(1)} = 0$ and $\Gamma_{2(1)} = 0$), as shown in Fig.2-(b)). Alternatively, the MZM can be coupled to one of the dots and the lead to the other, such that the MZM and dots are coupled in series ($t_{1(2)} = 0$ and $\Gamma_{2(1)} = 0$, see Fig.2-(c)).

A. MZM manipulation in non-interacting quantum dots

The non-interacting results for setups (a),(b) and (c) of Fig. 2 are shown in Figures 3, 4 and 5 respectively. In all cases, the left (right) panels depict the spectral density of dot 1 (dot 2). Each row represents a different gate voltage configuration in the dots, starting with $\epsilon_1 = \epsilon_2 = 0$ (first row), $\epsilon_1 = 5\Gamma_1$, $\epsilon_2 = 0$ (second row) and finally $\epsilon_1 = 0$, $\epsilon_2 = -5\Gamma_1$ (third row). The insets in each row shows where the Majorana signature, represented by a red dashed circle inside the dot, is mainly located.

Figure 3 shows results for the symmetric coupling

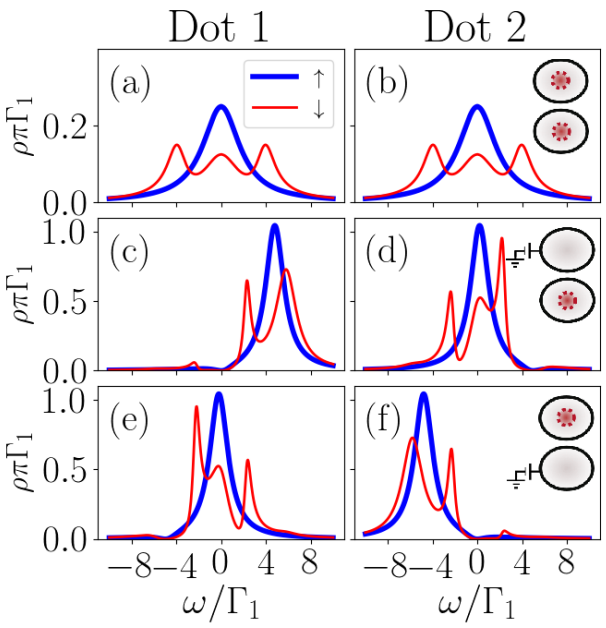

FIG. 3. Non-interacting LDOS in the symmetric coupling setup (Fig.2(a)) at each QD. First column: Dot 1. Second column: Dot 2. The gate voltages vary at each row. First row: Zero gate voltages $\epsilon_1 = \epsilon_2 = 0$. Second row: $\epsilon_1 = 5\Gamma_1$, $\epsilon_2 = 0$. Third row: $\epsilon_1 = 0$, $\epsilon_2 = -5\Gamma_1$. Bold blue lines: Spin-↑ LDOS. Thin red lines: Spin-↓ LDOS. The insets at the right show which dot carries a Majorana signature, represented by a red dashed circle. Upper: First dot. Lower: Second dot.

setup (Fig. 2(a)) in the non-interacting case. For the particle-hole symmetric case (first row), the LDOS for spin-↓ ($\rho_\downarrow(\omega)$, thin red line) and spin-↓ ($\rho_\uparrow(\omega)$, bold blue line) are identical in both dots, as expected. Notice, however, that the spin-↓ spectral densities (or LDOS) has a 3 peak structure, which is a consequence of the coupling with the Majorana mode. Moreover, the spin-↓ LDOS value at the Fermi energy is *half* of the respective spin-↑ LDOS value ($\rho_\downarrow(0) = \frac{1}{2}\rho_\uparrow(0)$), which signals the MZM tunneling into the dots. This Majorana signature is similar to the one observed when a single dot is coupled to a Majorana mode[15,16] and falls in our "type-II" category mentioned above. We thus may conclude that the MZM is delocalizing into both dots, as if in a "double slit" configuration.

More interesting, we find that such delocalization can be reversed (and thus manipulated) by applying gate voltages in the dots. If a positive or negative gate voltage is induced in one of the dots, the spin-↓ LDOS at the Fermi energy can vanish at that dot while the MZM signature ($\rho_\downarrow(0) = \frac{1}{2}\rho_\uparrow(0)$ remains in the other dot. This is shown in panels (c)-(f) of Fig. 3 for the case of positive (Fig. 3 c-d) and negative (Fig. 3 e-f) gate voltages.

The location of the MZM signature can also be controlled by quantum interference, as illustrated in panels (a) and (b) of Fig. 4. Here, the MZM is coupled directly only to dot 1, which is then coupled to the lead,

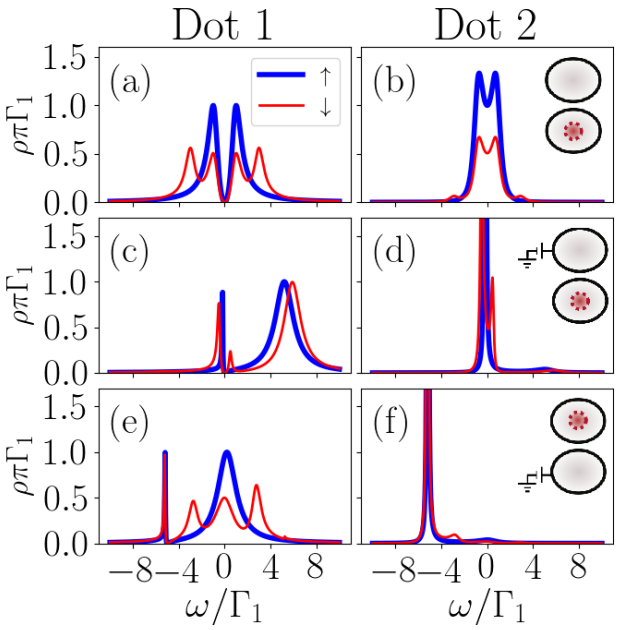

FIG. 4. The same as in Fig. 3 for the non-interacting LDOS of the setup in Fig.2(b)

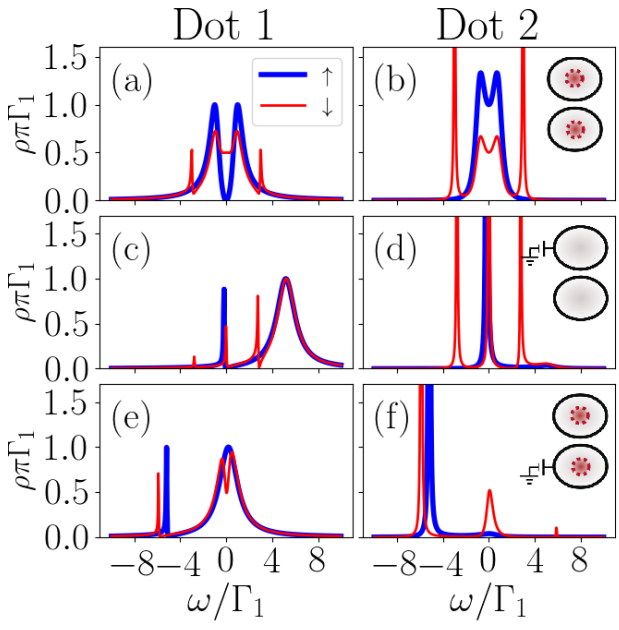

FIG. 5. The same as in Fig. 3 for the non-interacting LDOS of the set up in Fig.2(c) .

while dot 2 is coupled only to dot 1 via the inter-dot tunneling term ("side-dot" configuration, see Fig. 2-b). Interestingly, if the energy level of dot 2 is fixed to be in resonance with the Fermi energy of the lead, quantum interference causes the spectral function in dot 1 to *vanish* at the Fermi level (Fig. 4-a), while a type-I MZM signature ($\rho_\downarrow(0) = \frac{1}{2}\rho_\uparrow(0)$) appears in dot 2 only (Fig. 4-b). This interference-induced MZM signature in dot 2 is robust against shifts in dot 1's gate voltage, as depicted in Figs. 4-c & d. While dot 1's LDOS is pinned at zero at the Fermi energy, dot 2's spin-↓ LDOS exhibits a robust zero-mode of height $\frac{0.5}{\pi\Gamma}$, which is a type-II MZM signature.

This qualitative picture is radically altered when dot 2's gate voltage is shifted away from zero (Figs. 4(e)&(f)). In this case, dot 2 is no longer in resonance with the leads, which changes the interference conditions such that dot 1 spectral function is no longer pinned at zero. The plots clearly show that the MZM signature, previously located in dot 2, now appears in dot 1. Moreover, the spin-↑ and spin-↓ LDOS in dot 1 become very similar to the spectral densities observed in the case of a single dot[15,16], which indicates that dot 2 is essentially decoupled from the MZM.

Finally, we consider the "in series" configuration of Fig. 2(c), in which is similar to the "side-dot" configuration (Fig. 2(b)) except for the fact that the (spin-↓) MZM is coupled only to dot 2. Thus, results for the spin-↑ LDOS are identical to those shown in Fig. 4. However, the MZM signatures in the spin-↓ LDOS are quite distinct. As an example, when both dots are in resonance with the lead (Fig. 5(a) and (b)), the spin-↓ LDOS does not vanish at $\omega = 0$ as in the previous case. Instead, both dots show $(\rho_\downarrow(0) = \frac{0.5}{\pi\Gamma}$, which leads to MZM signatures of type-I in dot 2 and type-II in dot 1.

A shift in dot 1's gate voltage erases *both* MZM signatures, as shown in Figs. 5(c) and (d). Interestingly, the MZM signatures are robust against changes in the dot 2's gate voltage (Figs. 5(e) and (f) , but now the MZM signature types are switched: QD1 shows a type-I signature, which Q2 shows a type-II one.

B. MZM manipulation in interacting dots

We now turn to the more realistic case of quantum dots in the Coulomb blockade regime where local electron-electron interaction terms dominate the spectral function. We consider the dots to be in an odd-N Coulomb blockade valley where Kondo correlations are dominant at low-temperatures. The local Coulomb energy in the dots is accounted for by the terms $\frac{U_i}{2}(\sum_\sigma \hat{n}_{i\sigma} - 1)^2$ in Eq. (2). For simplicity, we consider equal Coulomb repulsion energies ($U_1 = U_2 \equiv U$) for both dots. For concreteness, the NRG calculations were performed with $U = 17.3\Gamma_1$ in both dots and a half-bandwidth of the lead electrons set at $D = 2U = 34.6\Gamma_1$.

Let us review some of the main features of the spectral densities of the dots in the absence of the MZM coupling. For a single dot coupled to a metallic lead, the Kondo effect is characterized by the appearance of a sharp resonance in the spectral function near the Fermi energy with a width of order $k_B T_K \sim \sqrt{U\Gamma_1}\exp\left[-\pi\frac{|\epsilon_1||\epsilon_1+U|}{U\Gamma_1}\right]$.

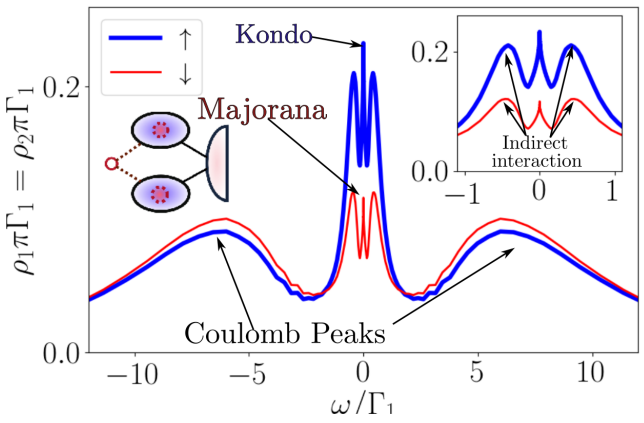

FIG. 6. Density of states of both dots in the symmetric coupling without gate voltages between the Majorana and the interacting DQD. Bold blue lines: Spin-↑ LDOS. Thin red lines: Spin-↓ LDOS. Inset: Low-energy LDOS.

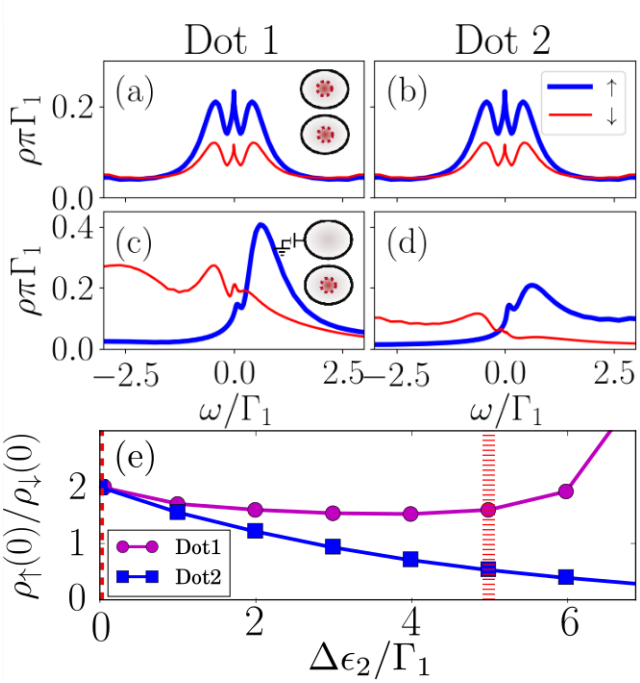

FIG. 7. The same as in Fig. 3 for the interacting LDOS in the symmetric coupling (Fig. 2(a)). (e): Evolution of $\frac{\rho_\downarrow(0)}{\rho_\uparrow(0)}$ vs increasing gate voltage $\Delta\epsilon_2$. Dash line: $\epsilon_2 = 0$ as in (a),(b). Bar line: $\epsilon_2 = 5\Gamma_1$ as in (c),(d).

Here, $T_K \ll U$ is the Kondo temperature of the system[27], which will be largest at the particle-hole symmetric point (phs) $\epsilon_1 = -\frac{U}{2}$. In the case of two dots at phs ($(\epsilon_{di} = -\frac{U_i}{2})$), both symmetrically coupled to a single lead, there will be an additional effective exchange interaction between the dots mediated by the lead Luis *Reference for this model?*. Such exchange will compete with the antiferromagnetic Kondo coupling, producing a three-peak structure in the spectral density of both dots.

Such exchange-driven three-peak structure remains when the MZM is coupled to the system in the symmetric coupling configuration (Fig. 2-(a)), as illustrated in Figure 6. At large energies, the spectral density displays Hubbard peaks at $\omega \sim \epsilon_{di} \pm 8.6\Gamma_1 = \pm\frac{U}{2}$ represent the single-particle hole- and electron-excitations and whose width is of order $\sim \Gamma_1$. In the spin up sector, the central peak three-peak structures represent the Kondo peak at $\omega = 0$ plus two satellite peaks at $\omega \sim \pm$...) Luis *What is the energy scale here?* Luis *Ok, we need to add that discussion on the atomic limit, remember? I would not call this RKKY. It is a hybridization between the dots!*

Moreover, the system presents a Majorana signature characterized by a type-I MZM signature $\rho_\downarrow(0) = \frac{1}{2}\rho_\uparrow(0)$. Note, that in this case the MZM signature coexists with the Kondo effect in the DQD as already predicted by Ruiz-Tijerina *et al.* for a single dot[18]. Both Kondo and MZM signatures occur in low-energy part of the spectral function $\omega \sim \Gamma_1$, as illustrated in the inset of Fig. 6. Within this scale, we can trace some interesting parallels with the non-interacting regime.

As an example, Fig. 7 shows the NRG results for the symmetric setup in Fig. 2(a). As in the non-interacting case (Fig. 3), type-I MZM signatures appear in both dots. These signatures can be manipulated by tuning one of the dot's gate voltage to induce the MZM to leak into the other dot. The LDOS at figures Fig. 7(d) shows a type-I Majorana signature with $\rho_\downarrow(0) \approx \frac{1}{2}\rho_\uparrow(0)$). This Majorana signature is stable for adjustments of energies bellow the $6\Gamma_1$ (see Fig. 7(e)). At larger gate voltages the coulomb peak at $\omega \sim 8.7$ overlaps with the Fermi energy which destroys both signals.

Luis *Stopped here. To be continued...*

In the second setup Fig. 2(b), the spin-↑ Kondo peak in Fig. 8 is destroyed by interference just as in the non-interacting case. This phenomenon had already been predicted for a T-junction of a double quantum dot attached to metallic leads[37]. The insight of our model is that an attached MZM should also disappear due to the same interference. Furthermore, a type I Majorana signature can be observed at very low energies in the inset of Fig. 8(b). However we have to recognize that both zero-modes decay significantly in the second dot. When the first voltage is turned on, the Majorana mode jumps onto the first dot which presents a type I Majorana signature. This is a clear difference with the non-interacting results where the Majorana signature stayed in the second dot. If the second dot is switched on , a type II Majorana signature appears a very low energies in dot 1, which is coherent with the idea that the Majorana interference should disappear in this case. In Fig. 8(e) we identify the emergy of a Fano resonance at the Fermi energy causing the sharp-asymmetric peak at $\omega = 0$.

Finally, Fig. 9 depicts the NRG results for the last configuration in Fig. 2(c). Notably, the indirectly-attached

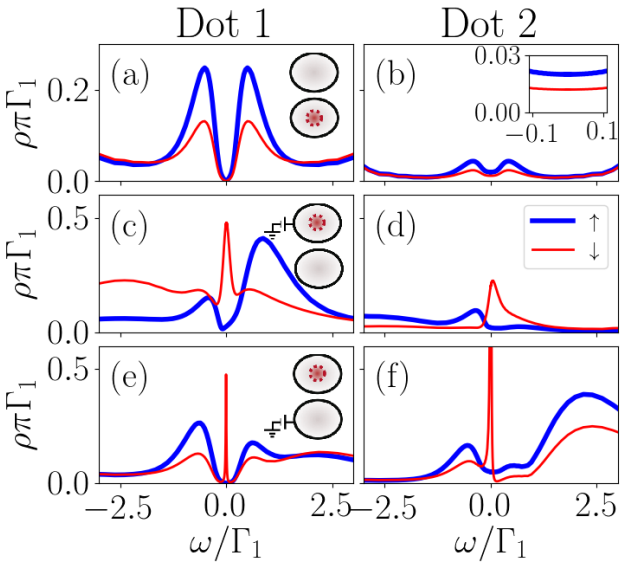

FIG. 8. The same as in Fig. 3 for the interacting LDOS of the setup in Fig.2(b). Inset in b): Low-energy LDOS.

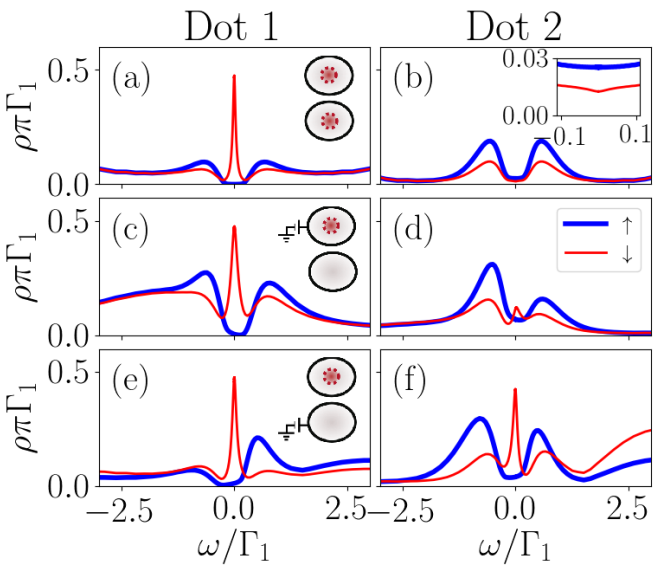

FIG. 9. The same as in Fig. 3 for the interacting LDOS of the set up in Fig.2(c) . Inset in b): Low-energy LDOS.

MZM exhibits a robust type II Majorana signature in the first dot over a destroyed Kondo peak. This signature is stable under the gate voltage tuning. In addition, only in the particle hole symmetric case the second dot presents a type II Majorana signature (Inset Fig. 9(b)). We could understand this effect by thinking that the QDs in model (c) are attached in series. Therefore the two dots can be thought as extensions of the Kitaev chain being the first dot the last place in the wire. Hence the Majorana should be localized at this dot despite the application of gate voltages. This case is similar to the case of a single dot attached to a Majorana chain, where it is known that the MZM appears in the dot even when this is supposed to be empty[16]. It still remains the doubt about why this effect is not observed in the non-interacting case . On the other hand, there is a significant zero-mode in the spin-↓ LDOS. This mode was not identified as a potential Majorana signature since it increases when $\Delta\epsilon_2$.

IV. CONCLUDING REMARKS

In this paper.... etc.

Comparing the exact analytical solution in the non-interacting system and the NRG results for interacting quantum dots, we were able to characterized the displacements of the MZM inside the double quantum dot for the three setups in Fig. 2. We observe a considerable agreement on the location of the Majorana signature between the interacting and non-interacting results:

Luis *No "itemize" in the Conclusions...* :

In the symmetric coupling the MZM leaks inside both dots (Fig. 2-a), we find that, for interacting dots, the Majorana signature will emerge near the Kondo temperature. At this regime the system presents combined Kondo-Majorana physics . Additional satellite peaks produced by the indirect exchange through the lead and the MZM appear at low energies. If the gate voltage of one dot is turned on the MZM is induced to tunnel only into the other dot.

In this system, the spin-↑ zero mode at QD1 (The Kondo peak if the system is interacting) is destroyed by quantum interference with the second dot, as shown in Fig. .2(b). This interference will also destroy the MZM in the first dot but a type I Majorana signature will still appear in the second dot. The Majorana mode can be induced to tunnel back into the first dot if a gate voltage is applied on the second dot. This signature is visible at very low energies (bellow $0.1\Gamma_1$) in interacting case.

An indirect type II Majorana signature is observed in the first dot, as represented in Fig 2(c). This signature is robust, specially in the interacting case, where it is present in all configurations.

ACKNOWLEDGMENTS

The authors thank Edson Vernek for enlightening discussions. L.G.G.V.D.S. acknowledges financial support by CNPq (grants No. 307107/2013-2 and 449148/2014-9), and FAPESP (grant No. 2016/18495-4).

Appendix A: Computation of the Green Function

In Zubarev's fermionic ballistic transport approach[25] the green function associated to two operators $A(t)$, $B(t)$ is defined as that Fourier transform of the time-ordered

anti-commutator of A and B

$$G_{A,B}(\omega) = \mathcal{F}\left\{\mathcal{T}\left[\{A(t), B(t')\}\right]\right\}(\omega)\,. \tag{A1}$$

The Fourier transform of Schrodinger evolution leads to transport equations of the

$$\omega G_{A,B}(\omega) = \delta_{A^\dagger,B} + G_{[A,H],B}(\omega). \tag{A2}$$

Applying this expression to Hamiltonian (1) replacing A and B by the creation and annihilation operators $d^\dagger_{i\sigma}, f^\dagger_\downarrow, c\dagger_{k\sigma}, d_{i\sigma}, f, c_{k\sigma}$ we obtain a linear transport system. We simplify the complexity of the equations by fixing $B = d^\dagger_{1\downarrow}$ and taking A as any other operator. In particular if A is equal to $f_\downarrow$ and $f^\dagger_\downarrow$ A2 becomes

$$(\omega - \epsilon_M)\, G_{f_\downarrow, d^\dagger_{1\downarrow}}(\omega) = \frac{t}{\sqrt{2}}\left(G_{d_{1\downarrow}, d^\dagger_{1\downarrow}}(\omega) - G_{d^\dagger_{1\downarrow}, d^\dagger_{1\downarrow}}(\omega)\right) \tag{A3}$$

$$(\omega + \epsilon_M)\, G_{f^\dagger_\downarrow, d^\dagger_{1\downarrow}}(\omega) = \frac{t}{\sqrt{2}}\left(G_{d_{1\downarrow}, d^\dagger_{1\downarrow}}(\omega) - G_{d^\dagger_{1\downarrow}, d^\dagger_{1\downarrow}}(\omega)\right). \tag{A4}$$

This allows us to take $G_{f^\dagger_\downarrow, d^\dagger_{1\downarrow}}(\omega) = \frac{\omega+\epsilon}{\omega-\epsilon} G_{f^\dagger_\downarrow, d^\dagger_{1\downarrow}}(\omega)$, allowing us to eliminate $G_{f^\dagger_\downarrow, d^\dagger_{1\downarrow}}(\omega)$ from the equations even before starting the Gauss-Jordan process.

Writing the other equations we obtain the linear system of the form

$$\mathcal{T}\vec{G}_{d^\dagger_1} = \hat{e}_1, \tag{A5}$$

where $\hat{e_1}$ is the vector with entries $\hat{e}_{1_n} = \delta_{1n}$, $\mathcal{T}$ is the transport matrix

$$\begin{bmatrix}
\omega-\epsilon_1 & -V_1^* & -t_{dots} & \frac{-t_1}{\sqrt{2}} & 0 & 0 & 0 \\
-V_1 & \omega-\epsilon_k & -V_2 & 0 & 0 & 0 & 0 \\
-t^*_{dots} & -V_2^* & \omega-\epsilon_2 & \frac{-t_2}{\sqrt{2}} & 0 & 0 & 0 \\
\frac{-\sqrt{2}t_1^*}{\omega+\epsilon_M} & 0 & \frac{-\sqrt{2}t_2^*}{\omega+\epsilon_M} & \omega-\epsilon_M & \frac{\sqrt{2}t_2^*}{\omega+\epsilon_M} & 0 & \frac{\sqrt{2}t_1^*}{\omega+\epsilon_M} \\
0 & 0 & 0 & \frac{t_2}{\sqrt{2}} & \omega+\epsilon_2 & V_2^* & t^*_{dots} \\
0 & 0 & 0 & 0 & V_2 & \omega+\epsilon_k & V_1 \\
0 & 0 & 0 & \frac{t_1}{\sqrt{2}} & t_{dots} & V_1^* & \omega+\epsilon_1
\end{bmatrix}, \tag{A6}$$

and $\vec{G}_{d^\dagger_1}$ is the column vector

$$\Big[G_{d_{1\downarrow}, d^\dagger_{1\downarrow}}(\omega), G_{c_{k\downarrow}, d^\dagger_{1\downarrow}}(\omega), G_{d_{2\downarrow}, d^\dagger_{1\downarrow}}(\omega), G_{f_\downarrow, d^\dagger_{1\downarrow}}(\omega),$$
$$G_{d^\dagger_{2\downarrow}, d^\dagger_{1\downarrow}}(\omega), G_{c^\dagger_{k\downarrow}, d^\dagger_{1\downarrow}}(\omega), G_{d^\dagger_{1\downarrow}, d^\dagger_{1\downarrow}}(\omega)\Big]^T.$$

The graph associated to matrix (A6) is the one in Fig. 10. Each vertex depicts the first subindex of the Green function. The "self-energies" inside each vertex are given by subtracting the corresponding diagonal term from ω . The weight at the edges is determined by the off-diagonal terms multiplied by -1.

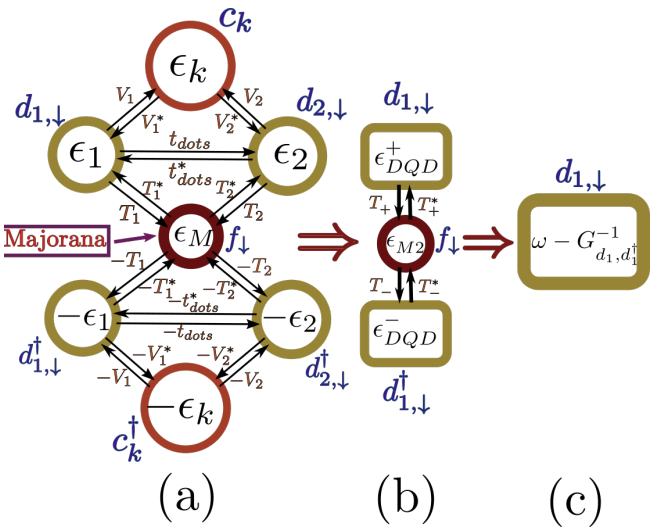

FIG. 10. Graph-Gauss-Jordan algorithm[31] applied to the DQD-Majorana model (a) Initial transport flow diagram (b) Graph obtained after popping vertexes $c_k, c^\dagger_k, d_{2,\downarrow}$ and $d^\dagger_{2,\downarrow}$. New couplings at (A11)-(A13) (c) Final graph after popping vertexes $f_\downarrow, d^\dagger_{1,\downarrow}$. The value of dot $d^\dagger_{1,\downarrow}$ depicts the self energy of the entire system $\omega - G_{d_{1\downarrow}, d^\dagger_{1\downarrow}}(\omega)$.

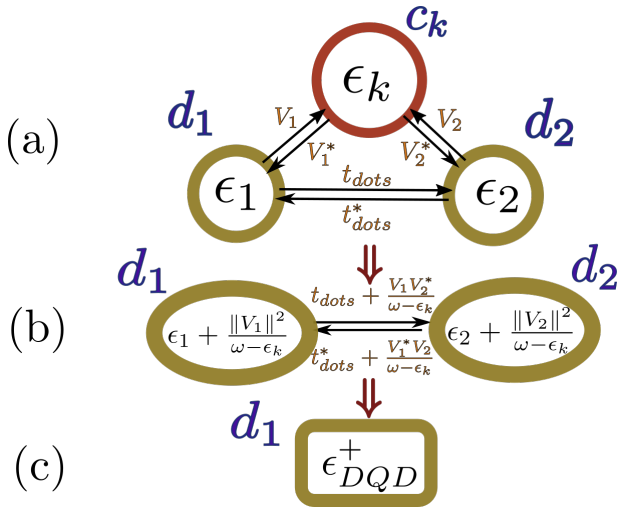

FIG. 11. Graph-Gauss-Jordan algorithm applied to a DQD attached to a lead. Since there is no Majorana, the spin index is not necessary. (a) Initial transport flow diagram (b) Graph obtained after popping vertex c_k . (c) Remaining vertex with self energy ϵ^+_{DQD} .

1. The double quantum dot

We will proceed to explain the Graph-Gauss-Jordan[31] elimination process in a simple DQD-model without Majorana fermions ($t_1 = t_2 = 0$). The transport matrix for

this system is

$$\begin{bmatrix} \omega-\epsilon_1 & -V_1 & -t_{dots} \\ -V_1^* & \omega-\epsilon_k & -V_2 \\ -t_{dots}^* & -V_2^* & \omega-\epsilon_2 \end{bmatrix}, \tag{A7}$$

which can be represented by the graph FIG11(a). To eliminate the vertex c_k we just need to subtract from (A7) the rank-1 matrix that cancels the row and the column corresponding to c_k. This matrix is

$$\begin{bmatrix} \frac{V_1^*V_1}{\omega-\epsilon_k} & -V_1^* & \frac{V_2V_1^*}{\omega-\epsilon_k} \\ -V_1 & \omega-\epsilon_k & -V_2 \\ \frac{V_2^*V_1}{\omega-\epsilon_k} & -V_2^* & \frac{V_2^*V_2}{\omega-\epsilon_k} \end{bmatrix}. \tag{A8}$$

The result of (A7) - (A8) is

$$\begin{bmatrix} \omega-\epsilon_1-\frac{V_1^*V_1}{\omega-\epsilon_k} & 0 & -t_{dots}-\frac{V_2V_1^*}{\omega-\epsilon_k} \\ 0 & 0 & 0 \\ -t_{dots}^*-\frac{V_2^*V_1}{\omega-\epsilon_k} & 0 & \omega-\epsilon_2-\frac{V_2V_1^*}{\omega-\epsilon_k} \end{bmatrix} \tag{A9}$$

which is depicted by the graphs in Fig. 11(b). Note that it is possible to associate the correction to the the energies and couplings to the possible walks passing through the vertex c_k. For instance d_1's energy ϵ_1 receives an extra-term $\frac{V_1^*V_1}{\omega-\epsilon_k}$ representing an additional walk from d_1 to d_1 passing through c_k. The same logic can be applied to the coupling terms. The correction to t_dots is $\frac{V_1^*V_2}{\omega-\epsilon_k}$ which corresponds to a path from d_1 to d_2 passing through the popped vertex c_k. Note that this term includes the multiplication both couplings with the vertex divided by the difference of ω with the energy of the vertex. This correspondence between the energy correction and eliminated paths through the graph makes the "popping" process an straightforward task.

The next step is to pop-out the vertex d_2 following the same procedure. At the end, the "self-energy" inside vertex d_1 will be

$$\epsilon^+_{DQD} = \epsilon_1 + \sum_{\mathbf{k}} \frac{V_1V_1^*}{\omega-\epsilon_{\mathbf{k}}} + \frac{\left\| t_{dots} + \sum_{\mathbf{k}} \frac{V_1V_2^*}{\omega-\epsilon_{\mathbf{k}}} \right\|^2}{\omega-\epsilon_2-\sum_{\mathbf{k}} \frac{V_2V_2^*}{\omega-\epsilon_{\mathbf{k}}}} \tag{A10}$$

and the green function of $G_{d_1d_1^\dagger}(\omega)$ in a DQD is symply $\frac{1}{\omega-\epsilon_{DQD}}$ (see Fig. 11(c)).

2. Solution of the general model

The previous algorithm to compute the Green function $G_{d,d\dagger}(\omega)$ of an operator d can be summarized to the following steps:

1. Computing the transport equations with the second term of the Green function fixed in the creation operator $d^\dagger$ at all equations.
2. Setting up the graph associated to the transport system. The self-energy of each vertex is initialized as ω minus the corresponding diagonal term. The edge weights are given by the coupling of the off-diagonal terms multiplied by -41.
3. Popping out the vertexes of the graph. Each popping process carries the following steps.
   (a) Computing the extra-terms of the energies and couplings based on the walks passing through the popped vertex.
   (b) Eliminating this vertex from the graph.
   (c) Iterating till there is only one vertex.
4. The energy in the remaining vertex d is the self-energy $\epsilon_d = \omega - \frac{1}{G_{d,d^\dagger}(\omega)}$.

Following these steps it is possible to solve the general case. We start with the graph in Fig. **??**(a) and we pop out the vertexes $c_k, c_k^\dagger, d_{2,\downarrow}$ and $d_{2,\downarrow}^\dagger$ in that order (See Fig. **??**(b)). The energies associated to $d_{1,\downarrow}$ and $d_{1,\downarrow}^\dagger$ will be similar to (A10) obtaining

$$\epsilon^\pm_{DQD} = \pm\epsilon_1 + \sum_{\mathbf{k}} \frac{V_1V_1^*}{\omega-\epsilon_{\mathbf{k}}} + \frac{\left\| \pm t_{dots} + \sum_{\mathbf{k}} \frac{V_1V_2^*}{\omega-\epsilon_{\mathbf{k}}} \right\|^2}{\omega\pm\epsilon_2-\sum_{\mathbf{k}} \frac{V_2V_2^*}{\omega-\epsilon_{\mathbf{k}}}}. \tag{A11}$$

There is also a correction in the couplings between the Majorana mode and $d_{1,\downarrow}$, $d_{1,\downarrow}^\dagger$ given by

$$T_\pm = \pm t_1 \pm t_2 \frac{\left(\pm t_{dots} + \sum_{\mathbf{k}} \frac{V_1V_2^*}{\omega-\epsilon_{\mathbf{k}}} \right)}{\omega\pm\epsilon_2\pm\sum_{\mathbf{k}} \frac{V_2V_2^*}{\omega-\epsilon_{\mathbf{k}}}}. \tag{A12}$$

Finally since the Majorana is in contact with dot 2, there is an extra-term appearing in the Majorana self energy given by

$$\epsilon_{M2} = \omega - \epsilon_M - \frac{\frac{\omega}{\omega+\epsilon_M}\|t_2\|^2}{\omega-\epsilon_2-\sum_{\mathbf{k}} \frac{V_2V_2^*}{\omega-\epsilon_{\mathbf{k}}}} - \frac{\frac{\omega}{\omega+\epsilon_M}\|t_2\|^2}{\omega+\epsilon_2-\sum_{\mathbf{k}} \frac{V_2V_2^*}{\omega+\epsilon_{\mathbf{k}}}}. \tag{A13}$$

With all the terms of the graph in Fig. **??**.(b) computed, it only remains to pop out vertexes $d_1^\dagger$ and $f_\downarrow$ in that order to obtain the result in equation (10).

$$G_{d_{1\downarrow},d_{1\downarrow}^\dagger}(\omega) = \frac{1}{\omega-\epsilon^+_{DQD}-\frac{\|T_+\|^2}{\omega-\epsilon_{M2}-\frac{\|T_-\|^2}{\epsilon^-_{DQD}}}}. \tag{A14}$$

From this analytic expression we can compute rapidly dynamical quantities such as the density of states in the non-interacting regime. This allowed us to predict interesting parameters for numerical simulations such as

in NRG which takes has a significant run-time. We introduced the Graph-Gauss-Jordan algorithm as a simple, didactic and graphical method to solve the equations of motion. We hope for its extended use in condensed matter physics.

[1] J. Alicea, Reports on Progress in Physics **75**, 076501 (2012).
[2] C. Beenakker, Annual Review of Condensed Matter Physics **4**, 113 (2013).
[3] A. Y. Kitaev, Physics-Uspekhi **44**, 131 (2001).
[4] A. Y. Kitaev, Annals of Physics **303**, 2 (2003), arXiv: quant-ph/9707021.
[5] V. Mourik, K. Zuo, S. M. Frolov, S. R. Plissard, E. P. a. M. Bakkers, and L. P. Kouwenhoven, Science **336**, 1003 (2012).
[6] A. Das, Y. Ronen, Y. Most, Y. Oreg, M. Heiblum, and H. Shtrikman, Nature Physics **8**, 887 (2012).
[7] M. T. Deng, C. L. Yu, G. Y. Huang, M. Larsson, P. Caroff, and H. Q. Xu, Nano Letters **12**, 6414 (2012).
[8] S. Nadj-Perge, I. K. Drozdov, J. Li, H. Chen, S. Jeon, J. Seo, A. H. MacDonald, B. A. Bernevig, and A. Yazdani, Science **346**, 602 (2014).
[9] M. T. Deng, S. Vaitiekenas, E. B. Hansen, J. Danon, M. Leijnse, K. Flensberg, J. Nygard, P. Krogstrup, and C. M. Marcus, Science **354**, 1557 (2016).
[10] H. Zhang, C.-X. Liu, S. Gazibegovic, D. Xu, J. A. Logan, G. Wang, N. van Loo, J. D. S. Bommer, M. W. A. de Moor, D. Car, R. L. M. Op het Veld, P. J. van Veldhoven, S. Koelling, M. A. Verheijen, M. Pendharkar, D. J. Pennachio, B. Shojaei, J. S. Lee, C. J. Palmstrm, E. P. A. M. Bakkers, S. D. Sarma, and L. P. Kouwenhoven, Nature **556**, 74 (2018).
[11] E. J. H. Lee, X. Jiang, R. Aguado, G. Katsaros, C. M. Lieber, and S. De Franceschi, Physical Review Letters **109**, 186802 (2012).
[12] D. Aasen, M. Hell, R. V. Mishmash, A. Higginbotham, J. Danon, M. Leijnse, T. S. Jespersen, J. A. Folk, C. M. Marcus, K. Flensberg, and J. Alicea, Physical Review X **6**, 031016 (2016).
[13] S. D. Sarma, M. Freedman, and C. Nayak, npj Quantum Information **1**, 15001 (2015).
[14] B. v. Heck, A. R. Akhmerov, F. Hassler, M. Burrello, and C. W. J. Beenakker, New Journal of Physics **14**, 035019 (2012).
[15] D. E. Liu and H. U. Baranger, Physical Review B **84** (2011), 10.1103/PhysRevB.84.201308, arXiv: 1107.4338.
[16] E. Vernek, P. H. Penteado, A. C. Seridonio, and J. C. Egues, Physical Review B **89**, 165314 (2014).
[17] M. Lee, J. S. Lim, and R. Lopez, Physical Review B **87**, 241402 (2013).
[18] D. A. Ruiz-Tijerina, E. Vernek, L. G. G. V. Dias da Silva, and J. C. Egues, Physical Review B **91**, 115435 (2015).
[19] G. Gorski, J. Baranski, I. Weymann, and T. Domanski, Scientific Reports **8**, 15717 (2018).
[20] M. Barkeshli and J. D. Sau, arXiv:1509.07135 [cond-mat, physics:quant-ph] (2015), arXiv: 1509.07135.
[21] T. Karzig, C. Knapp, R. M. Lutchyn, P. Bonderson, M. B. Hastings, C. Nayak, J. Alicea, K. Flensberg, S. Plugge, Y. Oreg, C. M. Marcus, and M. H. Freedman, Physical Review B **95**, 235305 (2017).
[22] J. F. Silva and E. Vernek, Journal of Physics: Condensed Matter **28**, 435702 (2016).
[23] T. I. Ivanov, Physical Review B **96**, 035417 (2017).
[24] Z. Su, A. B. Tacla, M. Hocevar, D. Car, S. R. Plissard, E. P. A. M. Bakkers, A. J. Daley, D. Pekker, and S. M. Frolov, Nature Communications **8**, 585 (2017).
[25] D. N. Zubarev, Soviet Physics Uspekhi **3**, 320 (1960).
[26] R. Bulla, T. A. Costi, and T. Pruschke, Reviews of Modern Physics **80**, 395 (2008).
[27] A. C. Hewson, *The Kondo Problem to Heavy Fermions* (Cambridge University Press, 1997) google-Books-ID: fPzgHneNFDAC.
[28] M. A. Ruderman and C. Kittel, Physical Review **96**, 99 (1954).
[29] T. Kasuya, Progress of Theoretical Physics **16**, 45 (1956).
[30] K. Yosida, Physical Review **106**, 893 (1957).
[31] D. A. Spielman, *Algorithms, Graph Theory, and Linear Equations in Laplacian Matrices*, Proceedings of the International Congress of Mathematicians (2010).
[32] K. G. Wilson, Reviews of Modern Physics **47**, 773 (1975).
[33] M. Sindel, *Numerical Renormalization Group studies of Quantum Impurity Models in the Strong Coupling Limit*, Text.PhDThesis, Ludwig-Maximilians-Universitt Mnchen (2005).
[34] W. Hofstetter, Phys. Rev. Lett. **85**, 1508 (2000).
[35] W. C. Oliveira and L. N. Oliveira, Physical Review B **49**, 11986 (1994).
[36] R. Peters, T. Pruschke, and F. B. Anders, Phys. Rev. B **74**, 245114 (2006).
[37] L. G. G. V. Dias da Silva, N. Sandler, K. Ingersent, and S. E. Ulloa, Physica E: Low-dimensional Systems and Nanostructures **40**, 1002 (2008).